nature structural & molecular biology

Structure of the VP16 transactivator target in the Mediator

Alexander G Milbradt[1], Madhura Kulkarni[2,3,5], Tingfang Yi[1,5], Koh Takeuchi[1,4], Zhen-Yu J Sun[1], Rafael E Luna[1], Philipp Selenko[1,4], Anders M Näär[2,3] & Gerhard Wagner[1]

The human Mediator coactivator complex interacts with many transcriptional activators and facilitates recruitment of RNA polymerase II to promote target gene transcription. The MED25 subunit is a critical target of the potent herpes simplex 1 viral transcriptional activator VP16. Here we determine the solution structure of the MED25 VP16-binding domain (VBD) and define its binding site for the N-terminal portion of the VP16 transactivation domain (TADn). A hydrophobic furrow, formed by a β-barrel and two α-helices in MED25 VBD, interacts tightly with VP16 TADn. Mutations in this furrow prevent binding of VP16 TAD to MED25 VBD and interfere with the ability of overexpressed MED25 VBD to inhibit VP16-dependent transcriptional activation *in vivo*. This detailed molecular understanding of transactivation by the benchmark activator VP16 could provide important insights into viral and cellular gene activation mechanisms.

Herpes simplex viruses (HSVs) usurp the host-cell transcriptional machinery upon infection to promote expression of viral genes[1]. Initial transcription of immediate-early (α) viral genes is activated by the tegument protein VP16 (also termed alpha-gene transactivating factor, α-TIF)[1]. VP16 possesses a potent transactivation domain (TAD) when fused to heterologous DNA-binding domains, and it has been suggested to be prototypic of 'acidic' TADs[2,3]. The molecular mechanism of transcription activation mediated by the VP16 TAD has thus been extensively studied to provide insights into more general mechanisms of gene activation[4].

Previously, we and others identified a large multiprotein complex that is required for transcriptional activation by VP16, as well as for other cellular and viral transcriptional activators, including nuclear receptors, the cholesterol and lipid regulator SREBP, the inflammation and apoptosis regulator NF-κB, adenoviral E1A 13S and the proto-oncoprotein p53 (refs. 5,6). This human transcription coactivator complex, which we initially termed activator-recruited cofactor (ARC), mediates activator-dependent recruitment of RNA polymerase II (Pol II) to target genes via binding to the C-terminal domain of the large Pol II subunit[7] (**Fig. 1**). It is structurally and functionally related to the *Saccharomyces cerevisiae* Mediator coactivator[8], and we therefore refer to it as the Mediator.

It is estimated that the Mediator coactivator complex comprises more than 30 subunits[9]. Growing experimental evidence suggests that many of these individual Mediator subunits can interact with transcriptional activators[10]. Previous studies by us and others indicated that the MED25 subunit (also known as ARC92 and ACID1) is a direct and functionally important target of the VP16 TAD[11,12] (**Fig. 1**). Notably, residues 402–590 of MED25 show high sequence homology to a repeated sequence in a protein of unknown function, PTOV1, that was previously identified based on its overexpression in prostate tumors[13] (**Supplementary Fig. 1a**). Moreover, deletion mutations showed that this MED25 region functioned as the VP16-binding domain (VBD), suggesting that this conserved sequence may represent a new activator binding motif[12] (**Supplementary Fig. 1a**). In our previous study, we also found that the N-terminal portion of the VP16 TAD (TADn, **Supplementary Fig. 1b**) is critical for strong interaction with MED25, whereas the C-terminal portion only mediated weak binding to MED25 (ref. 12). On the other hand, the C-terminal domain of the VP16 TAD has been found to recruit the histone acetyltransferases CBP and p300 (ref. 14). In addition, the C-terminal domain has also been reported to interact with the p62-Tfb1 subunit of TFIIH[15], with TAF9 (ref. 16) and with TFIIA to stimulate assembly of a TFIIA-TFIID–promoter complex[17]. The full-length VP16 TAD has been further shown to interact with TFIIB[18,19] and with PC4 (refs. 20,21). The latter interaction has been analyzed in detail[22]. Despite these advances, the precise molecular details of how VP16 activates transcription remain unclear.

Here we determined the solution structure of the 19 kDa MED25 VBD (residues 391–553) to consist of a seven-stranded β-barrel flanked by three α-helices. A hydrophobic groove formed by the β-barrel and two of the three α-helices serves as the VP16 TADn binding site. Point mutations targeting this groove prevent the full-length VP16 TAD from binding to MED25 VBD *in vitro* and abrogate dominant negative inhibition of VP16 TAD–dependent transcriptional activation by soluble MED25 VBD in cell culture studies.

Results from this study may have important ramifications for both viral and cellular mechanisms of gene activation. First, the newly

[1]Department of Biological Chemistry and Molecular Pharmacology, Harvard Medical School, Boston, Massachusetts, USA. [2]Massachusetts General Hospital Cancer Center, Charlestown, Massachusetts, USA. [3]Department of Cell Biology, Harvard Medical School, Boston, Massachusetts, USA. [4]Present addresses: Biomedical Information Research Center, National Institute of Advanced Industrial Science and Technology, Tokyo, Japan (K.T.), and Department of NMR-assisted Structural Biology, Leibniz Institute of Molecular Pharmacology, Berlin, Germany (P.S.). [5]These authors contributed equally to this work. Correspondence should be addressed to A.M.N. (naar@helix.mgh.harvard.edu) or G.W. (gerhard_wagner@hms.harvard.edu).

Received 18 May 2010; accepted 3 December 2010; published online 6 March 2011; doi:10.1038/nsmb.1999

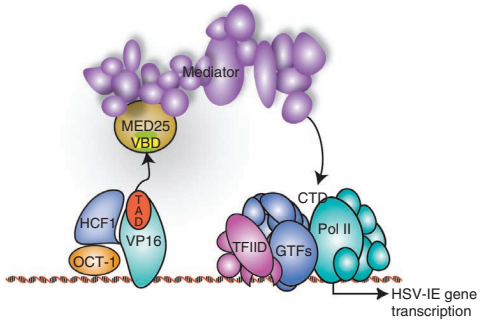

Figure 1 VP16-activated transcription. VP16, OCT-1 and HCF-1 form a VP16-induced complex[33]. The VP16 transactivation domain (TAD) interacts with the MED25 VP16 binding domain (VBD) to recruit the Mediator and activate transcription.

identified hydrophobic pocket on the surface of MED25 VBD could potentially serve as a new target for small-molecule inhibitors that impinge on MED25-dependent transcriptional activity by viral transactivators of the herpes family. These detailed structure-function studies will also guide future investigations elucidating the gene-activation mechanism of putative cellular transcriptional activators involved in Mediator recruitment through interactions with MED25 and its structurally conserved activator-binding domain.

RESULTS

Structure of MED25 VBD in solution

To obtain mechanistic insights into VP16 TAD–dependent transcriptional activation, we solved the three-dimensional solution structure of the MED25 VBD (amino acids 391–553, **Supplementary Fig. 1a**) by NMR spectroscopy. **Table 1** lists the statistics of the structure calculations. A summary of a Ramachandran plot generated by PROCHECK[23] is presented in **Supplementary Table 1**. **Supplementary Figure 2** shows a ^{1}H-^{15}N HSQC NMR spectrum with assigned peaks of the MED25 VBD. Procedures for sample preparation, data acquisition and structure calculation are described in the Online Methods section. The MED25 VBD shows a seven-stranded β-barrel flanked by three α-helices (**Fig. 2a**,**b**). The structure of the MED25 VBD contains large segments of high internal mobility that primarily localize to variable loops and to the unstructured N- and C termini of the protein (**Fig. 2a**,**b** and **Supplementary Fig. 3a**). The interior of the β-barrel is tightly packed with aromatic and aliphatic side chains. The barrel is capped by helix α2 on one side and by two adjacent loops at the opposite end of the structure (**Fig. 2b** and **Supplementary Fig. 3b**). Helices α1 and α3 are located on one side of the barrel. The placement of strands β1, β3, β5, the long loop between Glu410 and Leu423, and the C-terminal α3 helix creates a deep furrow that is lined with positively charged residues on both sides and hydrophobic residues at its base (**Fig. 2b**). The shape and charge distribution of the furrow, as well as the presence of a central prominent hydrophobic pocket of a size suitable for accommodating a hydrophobic or aromatic side chain, together suggest a potential peptide interaction site.

^{15}N T_2 relaxation measurements showed a relatively uniform distribution of ^{15}N T_2 relaxation times of approximately 50–60 ms (**Supplementary Fig. 3a**). The N- and C-terminal residues of MED25 VBD and the residues forming the long loop between β1 and β2 show substantially longer ^{15}N T_2 times, indicating higher local flexibility. Residues 500–508, constituting a loop between β5 and β6, show broad lines of amide resonances, which is most likely a result of local conformational exchange.

Notably, there are only two other human protein domains with considerable sequence homology to the MED25 VBD, both of which are present in PTOV1 (**Supplementary Fig. 1a**), a protein of unknown function that is overexpressed in prostate cancer[13]. The high degree of sequence homology suggests that the two PTOV1 domains could indeed undergo similar folding as the MED25 VBD; however, this will need to be experimentally confirmed.

A DALI search[24] identified three domains in the Protein Data Bank that have folds similar to the MED25 VBD (**Fig. 3** and **Supplementary Fig. 4**). However, they lack sequence homology to the MED25 VBD and have distinct chain topologies. The Spen paralog and ortholog C-terminal (SPOC) domain (PDB ID 1OW1)[25] is found in the Split ends (SPEN) family proteins, which regulate the expression of key transcriptional effectors in diverse signaling pathways. It was reported to mediate interactions with the silencing mediator for retinoid and thyroid receptors (SMRT) and the nuclear receptor co-repressor (NCoR) co-repressors; however, the precise function of this domain is unknown[25]. The other two structural homologs are found in the KU heterodimer (KU70–KU80) (PDB ID 1JEQ[26]), which is involved in double-stranded DNA repair[26]. Notably, all three structures lack the long C-terminal α3 helix that, together with β3 and β5, forms the hydrophobic pocket in MED25 VBD (**Figs. 2** and **3**). As our data discussed below indicate that the MED25 VBD hydrophobic pocket is critical for VP16 binding, this finding suggests that the structural homologs are unlikely to represent VP16 targets.

Molecular mechanism of MED25 VBD–VP16 TADn interaction

We tested two VP16 TAD constructs for binding to MED25 VBD (**Supplementary Fig. 1b**). A shorter, 42-residue fragment consisted of the N-terminal portion of the VP16 TAD (amino acids 411–452;

Table 1 NMR and refinement statistics for the MED25 VBD structure

	MED25 VBD
NMR distance and dihedral constraints	
Distance constraints	
Total NOE	1,755
Intra-residue	422
Inter-residue	1,333
Sequential ($\|i-j\|=1$)	546
Medium-range ($\|i-j\|<4$)	181
Long-range ($\|i-j\|>5$)	606
Hydrogen bonds	90
Total dihedral angle restraints	208
ϕ	104
ψ	104
Structure statistics	
Violations (mean and s.d.)	
Distance constraints (Å)	0.046 ± 0.0193
Dihedral angle constraints (°)	0.88 ± 0.480
Max. dihedral angle violation (°)	2.90
Max. distance constraint violation (Å)	0.26
Deviations from idealized geometry	
Bond lengths (Å)	0.011
Bond angles (°)	1.17
Impropers (°)	1.46
Average pairwise r.m.s. deviation[a] (Å)	
Heavy	0.75 ± 0.08
Backbone	0.49 ± 0.07

[a]Pairwise r.m.s. deviation was calculated among 25 refined structures. Values derived from the structured regions (**Supplementary Fig. 1a**) of the protein.

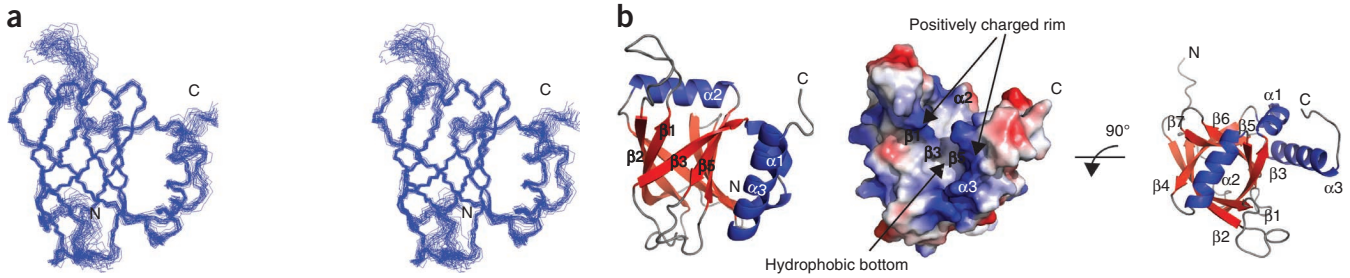

Figure 2 Solution structure of the MED25 VBD determined by NMR. (**a**) The 25 lowest-energy structures are shown overlaid using the secondary structure elements in side-by-side stereoview. (**b**) Cartoon drawing of MED25 VBD; the seven β-strands forming the barrel and the three α-helices are depicted in red and blue, respectively. The long α3 helix docks on the barrel by making close contact with β5, β6 and α1. Helix α2 caps the barrel from one side. A color-coded electrostatic surface potential shows a negative patch surrounded by areas of positive potential with a hydrophobic furrow in the center (**b**, middle panel), highlighted by arrows.

termed here TADn), and a longer 80-residue fragment contained the full-length TAD (amino acids 411–490; termed here TAD) (**Supplementary Fig. 1b**). Both peptides showed tight binding to MED25 VBD as determined by isothermal titration calorimetric (ITC) assays. The K_d of the VP16 TADn–MED25 VBD interaction was 1.6 μM (**Supplementary Fig. 5a**), whereas the full-length VP16 TAD binds to MED25 VBD with a K_d of approximately 50 nM (**Supplementary Fig. 5b**). The nanomolar affinity of the full-length VP16 TAD for the MED25 VBD is consistent with the notion that immobilized VP16 TAD can purify the Mediator complex from nuclear extracts in a single step[27].

We mapped the binding site of VP16 TADn on MED25 VBD and the binding site of MED25 VBD on VP16 TADn by NMR spectroscopy (**Fig. 4**). ^{1}H-^{15}N HSQC spectra of free VP16 TADn and TAD (**Fig. 4a**, blue signals, and **Supplementary Fig. 6a**) showed limited chemical shift dispersion, which is characteristic of unfolded polypeptide chains. In contrast to the free VP16 TADn and TAD, the ^{1}H-^{15}N HSQC spectra of the VP16 TADn (**Fig. 4a**, red signals, and **Supplementary Fig. 7**, red signals) and of the full-length TAD (**Supplementary Fig. 7**, black signals) in complex with the MED25 VBD showed new far-shifted NMR signals. The broad chemical shift dispersion of those signals indicated that the VP16 TAD adopts a partially folded conformation in the MED25 VBD–bound state. Moreover, a comparison of the spectra of the two bound peptides revealed an unexpected similarity in the far-shifted resonances, which suggested that the partially folded region was located in the TADn. (**Fig. 4a**, circled signals, and **Supplementary Fig. 7**, circled signals). The N-terminal VP16 TAD region was therefore identified as the primary MED25 VBD–binding portion. Consistent with this notion, a previous study showed that MED25-dependent transcriptional activation by the VP16 TAD required an intact TAD N terminus[12]. Based on the above-mentioned results, we used the N-terminal VP16 TAD construct (TADn) for all further NMR experiments and the full-length VP16 TAD (TAD) for pulldown and transcription activation assays.

We obtained sequential backbone assignment of free VP16 TADn by means of standard triple-resonance methods, whereas line broadening prevented us from obtaining continuous backbone resonances assignment of residues Ala434–Gly448 of bound VP16 TADn. In addition to triple-resonance backbone experiments, we used phenylalanine and leucine amino acid–selective labeling and ^{15}N dispersed NOESY spectra to obtain a nearly complete assignment of bound TADn amide resonances. Only residue Ala438 and Asp443 of bound TADn could not be assigned. Residues D439, D441, F442, L444, D445, L446, M447 and G448 of bound VP16 TADn experience major chemical shift changes upon binding to MED25 VBD (circled peaks in **Fig. 4a** indicated with assignment and highlighted bars in **Fig. 4c**) and may constitute a core binding segment of alternating hydrophobic and negatively charged residues (**Supplementary Fig. 1b** shows a conserved region in the TADn between Asp437 and Gly448). In addition, Phe442 of the VP16 TADn was shown to be of critical importance for the interaction with the MED25 VBD, as a point mutation of Phe442 to proline prevented binding of the TADn to the VBD[11].

^{1}H-^{15}N HSQC spectra of MED25 VBD showed substantial chemical shift changes upon addition of the VP16 TADn (**Fig. 4b**). The complex was in fast to intermediate exchange on the NMR time scale with regard to the dissociation kinetics, and it shuttled among multiple bound conformations, as discussed below. In order to locate the VP16 TADn–binding site on the MED25 VBD, we obtained greater than 90% of the backbone assignment of MED25 VBD bound to VP16 TADn and measured the magnitude of chemical shift changes of the ^{1}H-^{15}N HSQC cross peaks upon addition of the VP16 TADn peptide. The values are plotted versus the protein sequence in **Fig. 4d**. The most prominent chemical shift changes localized to a few discrete regions of the VBD that included residues T424, I449, Q451, I453, S468, C497, C499, L513 and H544. In a structural context, the strongest effects were observed for amino acids in β3 (**Fig. 4d**,**e**) and, to a lesser extent, β1, β5 and helices α1 and α3. Together, these structural elements form a patch of positively charged and hydrophobic residues that are likely to

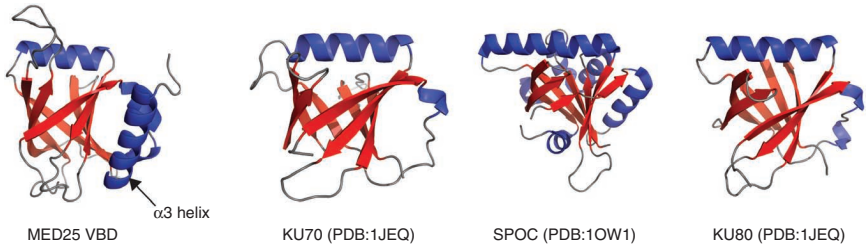

Figure 3 MED25 VBD adopts a rare seven-strand β-barrel fold. Cartoon drawing of MED25 VBD accompanied by three structural homologs found using DALI[34]: two β-barrel-domains from the KU70–KU80 complex (PDB 1JEQ[26]) and the SPOC (PDB 1OW1)[25] domain of SPEN. The three homologous structures have a different topology and lack the C-terminal helix present in MED25 VBD. The three MED25 VBD homologs are shown from left to right in decreasing degree of structural homology.

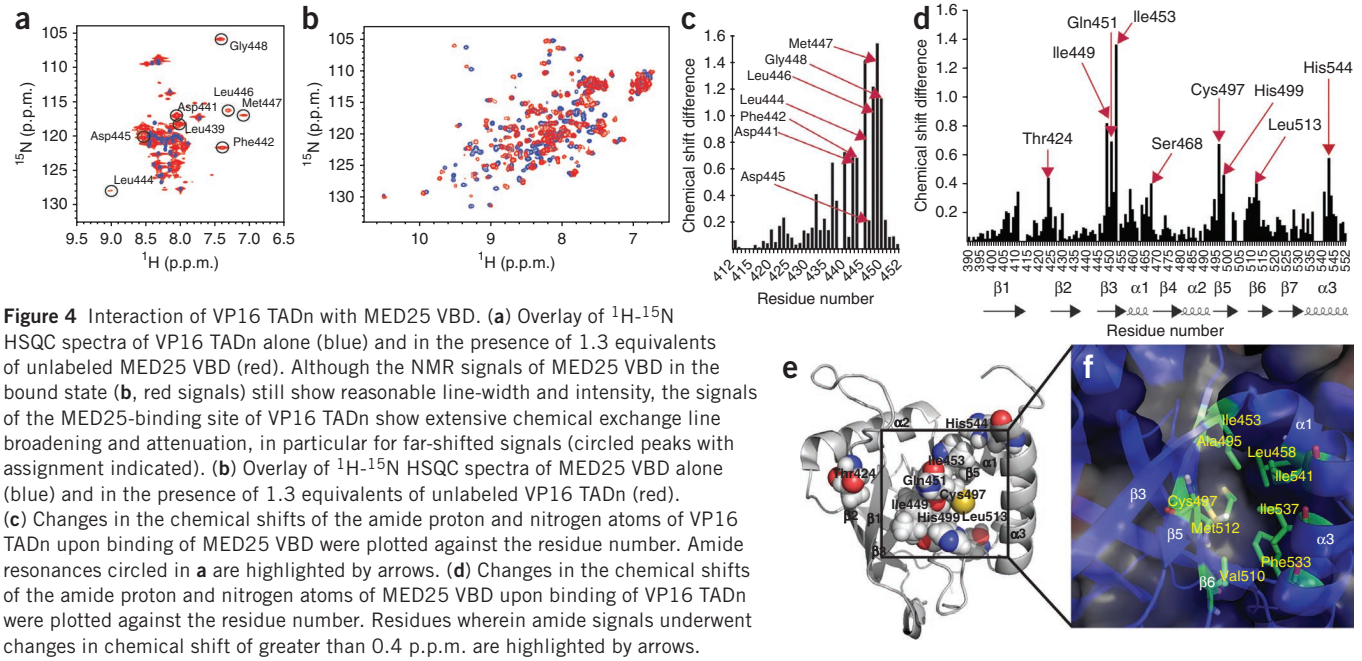

Figure 4 Interaction of VP16 TADn with MED25 VBD. (**a**) Overlay of ^{1}H-^{15}N HSQC spectra of VP16 TADn alone (blue) and in the presence of 1.3 equivalents of unlabeled MED25 VBD (red). Although the NMR signals of MED25 VBD in the bound state (**b**, red signals) still show reasonable line-width and intensity, the signals of the MED25-binding site of VP16 TADn show extensive chemical exchange line broadening and attenuation, in particular for far-shifted signals (circled peaks with assignment indicated). (**b**) Overlay of ^{1}H-^{15}N HSQC spectra of MED25 VBD alone (blue) and in the presence of 1.3 equivalents of unlabeled VP16 TADn (red). (**c**) Changes in the chemical shifts of the amide proton and nitrogen atoms of VP16 TADn upon binding of MED25 VBD were plotted against the residue number. Amide resonances circled in **a** are highlighted by arrows. (**d**) Changes in the chemical shifts of the amide proton and nitrogen atoms of MED25 VBD upon binding of VP16 TADn were plotted against the residue number. Residues wherein amide signals underwent changes in chemical shift of greater than 0.4 p.p.m. are highlighted by arrows. (**e**) A cartoon representation of MED25 VBD shows the clustering of the residues undergoing chemical shifts changes greater than 0.4 p.p.m. (drawn with space-filling spheres) upon interaction with VP16 TADn in or near the hydrophobic furrow. The changes are clustered on β3, β5, β6 and α3. (**f**) Residues Ile453, Leu458, ALa495, Cys497, Val510, Met512, Phe533, Ile537 and Ile541 of MED25 VBD form a central hydrophobic pocket with in the large hydrophobic furrow. Several residues in or near this pocket showed the most pronounced chemical shift changes upon binding of VP16 TADn (**Fig. 4e**).

engage in charge-charge and hydrophobicity-complementary interactions with amino acids of the VP16 TADn. A hydrophobic pocket formed by MED25 VBD residues Gln451 and Ile453 of β3, Ala495 and Cys497 of β5, Phe533, Ile537 and Ile541 of α3 and Leu458 of α1 lie at the core of the VP16 binding site (**Fig. 4f**). Indeed, the strongest overall chemical-shift changes upon binding of VP16 TADn were shown by MED25 VBD residues that are situated close to or within this hydrophobic pocket (**Fig. 4e**,**f**).

Both proteins showed exchange broadening of NMR resonances in the complex. Upon addition of VP16 TADn, residues Leu449, Gln451 and Ile453 of the MED25 VBD showed line broadening, and residues Arg538–Ile541 could not be assigned at all. On the side of VP16 TADn, residues Val431 to Gly448 showed extensive line broadening upon binding to MED25 VBD, and Ala438 and Asp443 could not be assigned. These observations indicate that there are likely multiple bound conformations. We have previously analyzed a similar situation in detail, in which we experimentally saw both phenomena: simple on-off binding and interaction with multiple bound states[28].

In addition, we found evidence that the C-terminal portion of the VP16 TAD (TADc) interacts with a portion of MED25 VBD that is opposite on the barrel to the binding site of TADn. By comparing ^{1}H-^{15}N HSQC spectra of the MED25 VBD, either bound to the TADn (**Supplementary Fig. 8a**, red signals) or bound to the full-length TAD (**Supplementary Fig. 8a**, black signals), one can monitor differences in the chemical shift of several amide resonances. Even without assignment of the MED25 VBD while it is bound to the TAD, we could identify five distinct changes in amide chemical shifts and infer their assignment from the MED25 VBD bound to the TADn. We concluded that the observed changes are caused by the interaction of the C-terminal domain of VP16 TAD with MED25 VBD and mapped them to residues Gln456, Val471, Ile521, Gly524 and Leu525 of the VBD. Because Ile521, Gly524 and Leu525 are located on β7 and Val471 is located on β4, the TADc binding site is distinct from the TADn binding site (**Supplementary Fig. 8b**). Gln456 is located on α1 and is possibly in contact with a hinge region of TAD. The interaction of TADn with β3 and β5 and the binding of TADc to β4 and β7 result in the VP16 TAD clamping the MED25 VBD.

Point mutants impinge on MED25 VBD–VP16 TAD interaction

Guided by the experimentally observed chemical shift changes on the VBD, we designed ten MED25 VBD point mutants with amino acid substitutions in the VP16 TAD binding site and in areas nearby. Because both positively charged and hydrophobic interactions are thought to contribute to the MED25 VBD–VP16 TAD binding site, we aimed to disrupt the interaction by uniformly replacing all residues with glutamic acid. We screened all mutants in pulldown assays in which lysates from either wild-type or mutant MED25 VBD–expressing HEK293T cells were added to immobilized full-length VP16 TAD. Fractions of bound MED25 VBD protein were then probed by immunoblotting. Only the MED25 VBD Q451E mutant failed to bind to VP16 TAD *in vitro*, whereas several other mutants (such as K447E, H499E and K545E) showed considerably lower binding than wild-type MED25 VBD (**Fig. 5a**). Subsequent NMR analyses confirmed that the Q451E mutant MED25 VBD indeed failed to interact with the VP16 TADn in solution, despite the fact that it remained properly folded (data not shown).

It has been shown previously that overexpressed, soluble MED25 VBD can prevent VP16 TAD–mediated transcriptional activation in a Gal4p-UAS transcription assay in human cells[12]. We therefore tested the four most attenuated binding mutants, K447E, Q451E, H499E and K545E, for their ability to inhibit full-length VP16 TAD–mediated transcription in HEK293T cells. Indeed, as expected from the binding studies, all four MED25 VBD mutants were unable to interfere with Gal4p-VP16 TAD–activated transcription in a dominant negative manner, as compared to wild-type MED25 VBD (**Fig. 5b**). Mutant and wild-type MED25 VBD showed a comparable level of expression when transfected into HEK293T cells (**Supplementary Fig. 9**).

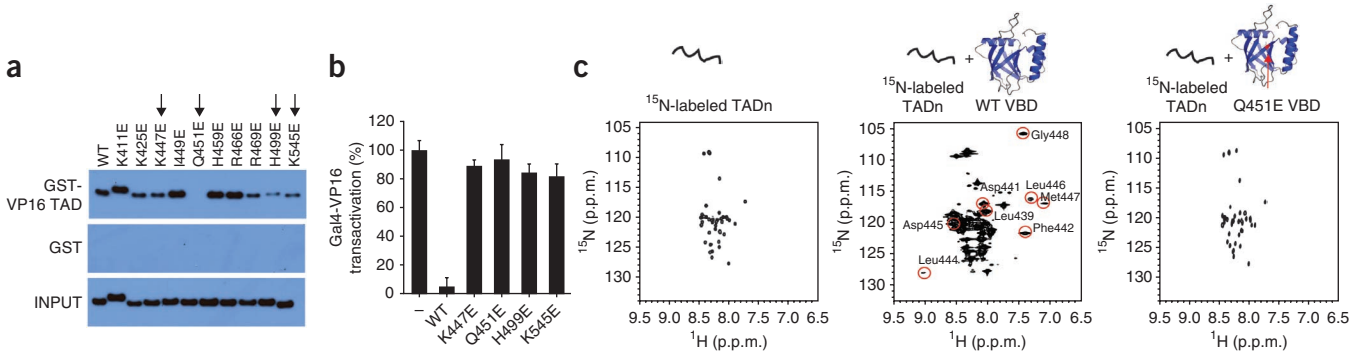

Figure 5 Functional studies of mutant MED25 VBD. (**a**) VP16 full-length TAD pulldown assays with MED25 VBD mutants. K447E, Q451E, H499E and K545E-mutated MED25 VBD shows weak or no binding to VP16 TAD (marked with an arrow). (**b**) Whereas wild-type MED25 VBD acts in a dominant negative fashion to inhibit Gal4p-VP16 full-length TAD-dependent transcription, the K447E, Q451E, H499E and K545E-mutated MED25 VBDs are incapable of inhibiting VP16-mediated transcription (WT: $P < 0.01$, *t*-test, one tailed, error bars represent s.d.). (**c**) The MED25 VBD Q451E mutation on β3 adjacent to the hydrophobic pocket disrupts binding of VP16 TADn to MED25 VBD. ^{1}H-^{15}N HSQC spectra of free VP16 TADn (left), at 1:1.3 excess of wild-type MED25 VBD (middle) and with 1:1.5 excess of Q451E MED25 VBD (right) show that VP16 TADn binds only loosely—as seen by minor chemical shift changes—to mutant MED25 VBD, without adopting a folded conformation. All far-shifted signals caused by the addition of wild-type MED25 VBD (middle, circled in red with assignment indicated) are missing when the mutant MED25 VBD is added to ^{15}N-labeled VP16 TADn (right).

NMR titrations of the unlabeled Q451E mutant MED25 VBD and ^{15}N-labeled VP16 TADn showed features of a remnant, substantially reduced interaction. Although minor chemical-shift changes were observed, all of the broadly dispersed resonances, characteristic of the partial folding transition of VP16, were absent (compare right and middle panels of **Fig. 5c**). We conclude that Q451E, sitting at the center of the hypothetical VP16 TADn binding site, greatly compromised the ability of MED25 VBD to interact with the viral peptide, both *in vitro* and *in vivo*.

DISCUSSION

The human Mediator coactivator complex is recruited by a number of viral and cellular transcription factors[10]. Previous studies by the authors and others have shown that the herpes simplex viral transactivator VP16 targets the Mediator by interacting with the MED25 subunit, and deletion mutagenesis has demonstrated that the MED25 VP16-binding domain is able to inhibit VP16-mediated transcriptional activation *in vivo*[11,12]. Our studies described here reveal the structure of the MED25 VBD and provide critical molecular details of the VP16 TAD–MED25 VBD interface. Our results also define an extended hydrophobic furrow on the MED25 VBD that is lined with positively charged residues, and we present evidence that amino acids located in this furrow play a key role in VP16 TAD binding and VP16 TAD–dependent transcriptional activation. Indeed, our results show that a single MED25 VBD mutation (Q451E) located in a central hydrophobic pocket within the furrow prevents binding to the VP16 TAD *in vitro* and abolishes the dominant negative inhibition of MED25 VBD on VP16 TAD–dependent transcriptional activation in cellular contexts.

Although several other entries in the Protein Data Bank (such as the SPOC domain of SPEN and the two β-barrel structures of the KU70–KU80 heterodimer) show superficial structural homology to the MED25 VBD (**Fig. 3**), they present different folding topologies and lack the long C-terminal helix α3. Because α3 together with β3 and β5 form part of the hydrophobic VP16-binding pocket, these differences suggest that the MED25 VBD represents a structurally and functionally distinct domain and that these other proteins are unlikely targets of VP16 or other viral transactivators of the herpes family.

Multiple sequence alignments indicate that residues in the hydrophobic pocket are well conserved among the N- and C-terminal domains of PTOV1 and MED25 VBD (**Supplementary Fig. 1a**). Although we have previously shown that the VP16 TAD does not associate with PTOV1 when expressed in cells[12], our structural studies of MED25 VBD and its extensive conservation with the two PTOV1 domains suggest that PTOV1 could indeed represent a target for both viral and cellular transcription factors. Because PTOV1 was first identified as a putative prostate cancer oncogene[13], it is tempting to speculate that PTOV1 (and the MED25 VBD–related domains) may play a role as a target for cellular activators in gene regulatory pathways contributing to prostate cancer proliferation.

The VP16 TADn peptide adopts a folded conformation upon binding to MED25 VBD, while retaining a certain degree of flexibility. We conclude from titration experiments that VP16 TADn samples two or more conformations in the bound state, consistent with an 'induced fit' type of interaction. This intrinsically unfolded structure of the unliganded state of the VP16 TADn may allow a multitude of interactions with transcriptional targets. Indeed, whereas a single bound state may provide the tightest association, strong interaction with one partner might prevent binding to additional coactivator partners (for example, CBP-p300), impeding efficient transactivation. Accordingly, as shown in previous studies, the VP16 TAD interacts with a number of targets in the basal transcription machinery, including TFIIB[18,19], TFIIA[17], the TFIID subunit $TAF_{II}31$ (ref. 16) and the Tfb1 subunit of TFIIH[15].

Notably, other viral activators of the herpes family also employ MED25 and its VP16-binding domain as their transcription regulatory conduit. Indeed, both the varicella-zoster virus IE62 protein and the Kaposi's sarcoma–associated herpesvirus LANA-1 protein target MED25 (refs. 29,30), and IE62 was shown to directly interact with the same region of MED25 as VP16 (ref. 31). Taken together with the findings presented here, as well as those of previous studies by the authors and others[11,12], these results indicate that MED25 and the VP16-binding domain could serve a critical role in transactivation of viral genes in the herpes family of viruses, and the molecular interface of viral activators and MED25 might thus provide a new target for the development of antiviral therapeutics.

Viruses commonly mimic, or hijack, cellular mechanisms for their maturation and propagation. It is therefore likely that cellular transactivators also target MED25 and the VP16-binding domain that we have structurally defined here for transcriptional regulation. In this

regard, it is noteworthy that MED25 has been implicated in Charcot-Marie-Tooth neuropathy[32], in which it has been suggested to play an as yet poorly understood pathophysiological role in gene activation.

In conclusion, our study has revealed intricate structural and mechanistic details of the gene activation mechanism of the benchmark activator VP16 that might guide future investigations of transactivation mechanisms of both viral and cellular activators. These studies could also provide insights and tools to design new therapeutic strategies that target the molecular underpinning of viral transactivation that is essential to propagation of herpes family viruses.

METHODS

Methods and any associated references are available in the online version of the paper at http://www.nature.com/nsmb/.

Accession codes. The coordinates for the structure of MED25 VBD have been deposited in the Protein Data Bank with the accession code 2KY6. Biological Magnetic Resonance Bank: The chemical shifts were deposited under entry 17139.

Note: Supplementary information is available on the Nature Structural & Molecular Biology website.

ACKNOWLEDGMENTS

We thank M. Oberer for initial NMR data collection, R. Rodriguez for critical advice on designing biochemical experiments, K. Edmonds for critical reading and Python script writing, S. Hiller and V. Orekhov for advice and assistance with nonlinear-sampling NMR data collection and processing, and H. Arthanari for advice on NMR data collection and manuscript editing. We are very grateful to M. Sattler and E. Vojnic of the Technical University of Munich for critical discussion of unpublished data. We are also thankful for H.C. Seou's assistance with DNA cloning procedures and A. Koglin for help with CNS calculations. A.G.M. was partially supported by a Deutscher Akademischer Austausch Dienst postdoctoral fellowship. P.S. was funded by the Human Frontier Science Program Organization long-term fellowship LT00686/2004-C. The work was supported by US National Institutes of Health grants CA127990 (G.W. and A.M.N.), GM47467 and EB002026 (G.W.) and GM071449 (A.M.N.).

AUTHOR CONTRIBUTIONS

A.G.M. prepared protein samples, recorded and analyzed NMR data, calculated the structure, designed the MED25 VBD mutants and co-wrote the paper; M.K. generated point mutations, did pulldown assays and assisted with transcription assays; T.Y. did transcription assays; R.E.L. assisted with transcription assays, data interpretation and writing of the paper; K.T. and P.S. cloned the original construct, collected initial NMR data, obtained preliminary assignment, and assisted with editing and writing the paper; Z.-Y.J.S. assisted in recording NMR data, data analysis and structure calculation; A.M.N. and G.W. initiated the project, helped design experiments, advised on data collection and interpretation, and participated in writing and editing the manuscript.

COMPETING FINANCIAL INTERESTS

The authors declare no competing financial interests.

Published online at http://www.nature.com/nsmb/.
Reprints and permissions information is available online at http://npg.nature.com/reprintsandpermissions/.

1. Roizman, B. & Knipe, D. in *Fundamental Virology*, 4th edn (eds. Knipe, D.M. *et al.*) 1123–1183 (Lippincott-Raven, 2001).
2. Triezenberg, S.J., Kingsbury, R.C. & McKnight, S.L. Functional dissection of VP16, the trans-activator of herpes simplex virus immediate early gene expression. *Genes Dev.* **2**, 718–729 (1988).
3. Greaves, R. & O'Hare, P. Separation of requirements for protein-DNA complex assembly from those for functional activity in the herpes simplex virus regulatory protein Vmw65. *J. Virol.* **63**, 1641–1650 (1989).
4. Ghosh, S., Toth, C., Peterlin, B.M. & Seto, E. Synergistic activation of transcription by the mutant and wild-type minimal transcriptional activation domain of VP16. *J. Biol. Chem.* **271**, 9911–9918 (1996).
5. Näär, A.M., Lemon, B.D. & Tjian, R. Transcriptional coactivator complexes. *Annu. Rev. Biochem.* **70**, 475–501 (2001).
6. Boyer, T.G., Martin, M.E., Lees, E., Ricciardi, R.P. & Berk, A.J. Mammalian Srb/Mediator complex is targeted by adenovirus E1A protein. *Nature* **399**, 276–279 (1999).
7. Näär, A.M., Taatjes, D.J., Zhai, W., Nogales, E. & Tjian, R. Human CRSP interacts with RNA polymerase II CTD and adopts a specific CTD-bound conformation. *Genes Dev.* **16**, 1339–1344 (2002).
8. Kornberg, R.D. Mediator and the mechanism of transcriptional activation. *Trends Biochem. Sci.* **30**, 235–239 (2005).
9. Conaway, R.C., Sato, S., Tomomori-Sato, C., Yao, T. & Conaway, J.W. The mammalian Mediator complex and its role in transcriptional regulation. *Trends Biochem. Sci.* **30**, 250–255 (2005).
10. Malik, S. & Roeder, R.G. Dynamic regulation of pol II transcription by the mammalian Mediator complex. *Trends Biochem. Sci.* **30**, 256–263 (2005).
11. Mittler, G. *et al.* A novel docking site on Mediator is critical for activation by VP16 in mammalian cells. *EMBO J.* **22**, 6494–6504 (2003).
12. Yang, F., DeBeaumont, R., Zhou, S. & Naar, A.M. The activator-recruited cofactor/Mediator coactivator subunit ARC92 is a functionally important target of the VP16 transcriptional activator. *Proc. Natl. Acad. Sci. USA* **101**, 2339–2344 (2004).
13. Benedit, P. *et al.* PTOV1, a novel protein overexpressed in prostate cancer containing a new class of protein homology blocks. *Oncogene* **20**, 1455–1464 (2001).
14. Ikeda, K., Stuehler, T. & Meisterernst, M. The H1 and H2 regions of the activation domain of herpes simplex virion protein 16 stimulate transcription through distinct molecular mechanisms. *Genes Cells* **7**, 49–58 (2002).
15. Langlois, C. *et al.* NMR structure of the complex between the Tfb1 subunit of TFIIH and the activation domain of VP16: structural similarities between VP16 and p53. *J. Am. Chem. Soc.* **130**, 10596–10604 (2008).
16. Uesugi, M., Nyanguile, O., Lu, H., Levine, A.J. & Verdine, G.L. Induced alpha helix in the VP16 activation domain upon binding to a human TAF. *Science* **277**, 1310–1313 (1997).
17. Kobayashi, N. *et al.* DA-complex assembly activity required for VP16C transcriptional activation. *Mol. Cell. Biol.* **18**, 4023–4031 (1998).
18. Hayashi, F. *et al.* Human general transcription factor TFIIB: conformational variability and interaction with VP16 activation domain. *Biochemistry* **37**, 7941–7951 (1998).
19. Hall, D.B. & Struhl, K. The VP16 activation domain interacts with multiple transcriptional components as determined by protein-protein cross-linking *in vivo*. *J. Biol. Chem.* **277**, 46043–46050 (2002).
20. Kretzschmar, M., Kaiser, K., Lottspeich, F. & Meisterernst, M. A novel mediator of class II gene transcription with homology to viral immediate-early transcriptional regulators. *Cell* **78**, 525–534 (1994).
21. Ge, H. & Roeder, R.G. Purification, cloning, and characterization of a human coactivator, PC4, that mediates transcriptional activation of class II genes. *Cell* **78**, 513–523 (1994).
22. Jonker, H.R., Wechselberger, R.W., Boelens, R., Folkers, G.E. & Kaptein, R. Structural properties of the promiscuous VP16 activation domain. *Biochemistry* **44**, 827–839 (2005).
23. Laskowski, R.A., Rullmannn, J.A., MacArthur, M.W., Kaptein, R. & Thornton, J.M. AQUA and PROCHECK-NMR: programs for checking the quality of protein structures solved by NMR. *J. Biomol. NMR* **8**, 477–486 (1996).
24. Holm, L. & Sander, C. Protein structure comparison by alignment of distance matrices. *J. Mol. Biol.* **233**, 123–138 (1993).
25. Ariyoshi, M. & Schwabe, J.W. A conserved structural motif reveals the essential transcriptional repression function of Spen proteins and their role in developmental signaling. *Genes Dev.* **17**, 1909–1920 (2003).
26. Walker, J.R., Corpina, R.A. & Goldberg, J. Structure of the Ku heterodimer bound to DNA and its implications for double-strand break repair. *Nature* **412**, 607–614 (2001).
27. Näär, A.M. *et al.* Composite co-activator ARC mediates chromatin-directed transcriptional activation. *Nature* **398**, 828–832 (1999).
28. Reibarkh, M., Malia, T.J. & Wagner, G. NMR distinction of single- and multiple-mode binding of small-molecule protein ligands. *J. Am. Chem. Soc.* **128**, 2160–2161 (2006).
29. Yang, M., Hay, J. & Ruyechan, W.T. Varicella-zoster virus IE62 protein utilizes the human mediator complex in promoter activation. *J. Virol.* **82**, 12154–12163 (2008).
30. Roupelieva, M. *et al.* Kaposi's sarcoma–associated herpesvirus Lana-1 is a major activator of the serum response element and mitogen-activated protein kinase pathways via interactions with the Mediator complex. *J. Gen. Virol.* **91**, 1138–1149 (2010).
31. Yamamoto, S., Eletsky, A., Szyperski, T., Hay, J. & Ruyechan, W.T. Analysis of the varicella-zoster virus IE62 N-terminal acidic transactivating domain and its interaction with the human mediator complex. *J. Virol.* **83**, 6300–6305 (2009).
32. Leal, A. *et al.* Identification of the variant Ala335Val of MED25 as responsible for CMT2B2: molecular data, functional studies of the SH3 recognition motif and correlation between wild-type MED25 and PMP22 RNA levels in CMT1A animal models. *Neurogenetics* **10**, 275–287 (2009).
33. Wysocka, J. & Herr, W. The herpes simplex virus VP16-induced complex: the makings of a regulatory switch. *Trends Biochem. Sci.* **28**, 294–304 (2003).
34. Holm, L. Unification of protein families. *Curr. Opin. Struct. Biol.* **8**, 372–379 (1998).

ONLINE METHODS

Luciferase assay. For luciferase assays, approximately 5×10^5 HEK293T cells were plated into each well of 24-well plates and cotransfected with/or without 0.5 μg of MED25 VBD expression vector (wild-type or one of the ten mutants), 100 ng of G4BE luciferase reporter, 5 ng of *Renilla* luciferase plasmid and 2 ng of HA-Gal4-VP16 expression vector. Transfected cells were lysed after 24 h and analyzed using the Dual Luciferase System (Promega).

Mutagenesis. In order to insert point mutations in our respective vectors, we employed the QuikChange Site-directed Mutagenesis kit from Stratagene, following the manufacturer's directions. Fully complementing primers (45-mer) containing nucleotide mutations within the middle of each primer were designed with an average of 18-mer flanking sequences. Primer sequences are provided upon request.

Protein expression and purification. The MED25 VBD (residues 390–553) was cloned into a pHis-Gb1-Parallel1 vector, a derivative of the pHis-Parallel1[35], using the EcoRI and KpnI cleavage sites. The construct was expressed in BL21(DE3) *Escherichia coli* cells. The cells were grown to an OD_{600} of 0.8 and induced with 1 mM IPTG for 3–5 h at 37 °C. Unlabeled proteins were grown in LB medium, labeled proteins were grown in M9 medium containing 1 g [^{15}N]NH_4Cl, 2 g [^{13}C]glucose or 2 g [^{2}H-^{13}C]glucose and D_2O for deuterated ^{13}C- and ^{15}N-labeled proteins. Cells were sonicated in 20 mM Tris-HCl, pH 8.0, 300 mM NaCl, 10 mM imidazole, 0.1% (v/v) Triton X-100, 1 mg ml^{-1} lysozyme, 2 mM β-mercaptoethanol and 1 tablet of Roche Complete Protease Inhibitor. The soluble fraction was obtained by centrifugation at 8,000*g* for 1 h. The supernatant was applied to a Ni-NTA resin and washed with 10 volumes of 20 mM Tris-HCl, pH 8.0, 300 mM NaCl, 10 mM imidazole and 2 mM β-mercaptoethanol and then eluted with 5 volumes 20 mM Tris-HCl, pH 8.0, 300 mM NaCl, 300 mM imidazole and 2 mM β-mercaptoethanol. The eluted protein was cleaved with TEV protease overnight at 4 °C. The reaction mixture was diluted to roughly 50 mM NaCl and further purified by ion-exchange chromatography on a Resource S column (GE Healthcare) in 20 mM sodium phosphate buffer, pH 6.5, 3 mM DTT with a linear NaCl gradient from 50 to 500 mM NaCl. VP16 TADn (411–452) and VP16 TAD (411–490) were cloned into a pETM30 vector using the NpnI and KpnI restriction sites. BL21(DE3) *E. coli* cells were transformed with the above-mentioned vector, grown to an OD_{600} of 0.8 and induced with 1 mM IPTG for 2–3 h at 37 °C. Unlabeled proteins were grown in LB medium and labeled proteins in M9 containing 1 g [^{15}N]NH_4Cl, 2 g [^{13}C]glucose or 2 g [^{2}H-^{13}C]glucose and D_2O for deuterated ^{13}C- and ^{15}N-labeled proteins. The MED25 VBD purification method with the subsequent TEV cleavage step was also used for VP16 TADn and TAD. After TEV cleavage, the protein solution was diluted to 1 mg ml^{-1} and subjected to a freeze-thaw cycle to precipitate glutathione *S*-transferase (GST). Precipitated GST was removed by centrifugation at 8,000*g* for 1 h. The remaining VP16 TADn or TAD peptide was concentrated and further purified by gel filtration on Superdex 75 (GE Healthcare) in 20 mM Tris-HCl, pH 8.0, 150 mM NaCl, 3 mM DTT and 0.25 mM EDTA. Protein concentrations were determined from the absorbance at 280 nm. An S411W mutant of VP16 TADn was used to facilitate determination of protein concentrations at 280 nm. [^{15}N]phenylalanine and [1-^{13}C]leucine ^{15}N (U) amino acid–selective labeled samples of TADn were prepared according to previously published work and references therein[36].

Nuclear magnetic resonance spectroscopy. All NMR samples were prepared in 20 mM sodium phosphate buffer, pH 6.5, 150 mM NaCl, 3 mM DTT. When VP16 TADn was present, 0.25 mM EDTA was added to the solution to prevent proteolytic degradation. Spectra were recorded on Varian Inova 500 and 600 and on Bruker 600, 750 and 900 MHz spectrometers at 25 °C. Resonance assignment was achieved by the use of standard multidimensional heteronuclear NMR-experiments[37]. NOEs were derived from 2D-^{1}H-^{1}H-NOESY, 3D ^{15}N-dispersed NOESY-HSQC, 3D ^{13}C-dispersed NOESY-HSQC and 4D HMQC-NOESY-HMQC experiments[38]. The mixing times were 60 ms for the 2D and 3D NOESYs and 150 ms for the 4D NOESY. The 4D NOESY was recorded on a ^{1}H-^{13}C methylisoleucine-, leucine- and valine-labeled sample with a deuterated protein background[39]. Spectra were processed with NMRpipe[40]. The sparsely sampled 4D NOESY was processed with the multi-dimensional decomposition (MDD) software[38] and subsequently with NMRpipe according to Hiller *et al.*[38]. Amino acid–selective labeled samples were recorded with HSQC spectra for ^{15}N-labeled phenylalanine samples or with ^{1}H-^{15}N planes of HNCO spectra[37] for [1-^{13}C]leucine ^{15}N (U)-labeled samples. NMR spectra were plotted with the programs Sparky 3 (http://www.cgl.ucsf.edu/home/sparky/) and CARA[41].

Structure calculation. NOEs were picked and assigned manually in CARA[41] or automatically derived from CYANA-CANDID[42]. Dihedral constraints were derived from C^{α} and C^{β} chemical shifts using the program TALOS+ (ref. 43). NOE intensities were integrated and converted into distance constraints using CYANA[42]. Hydrogen bond restraints for β-sheets and helices were assigned when supported by NOEs and secondary structure prediction. Fifty initial structures were created in a simulated annealing protocol using CYANA-CANDID[42]. The 25 structures with lowest energy were subsequently refined with CNS[44] using explicit solvent in a molecular dynamics simulation. Structures were visualized with the PyMOL Molecular Graphics System v.1.2r3pre (Schrödinger). Sequence alignments were visualized with ESPRIPT[45]. PSVS[46], CNS[44] and PROCHECK-NMR[23] were used for analysis of the structural ensemble and quality assessment of the structural data.

Isothermal titration calorimetry. Protein samples were prepared in 20 mM sodium phosphate, pH 6.5, 150 mM NaCl, 0.5 mM TCEP, 0.25 mM EDTA. A VP-isothermal titration calorimeter (MicroCal) was run at an equilibrium temperature of 25 °C. The concentration of the protein in the well was roughly ten times the estimated K_d and the concentration of the protein in the syringe was seven times the one in the well. Data were processed using Origin software (OriginLab).

Glutathione *S*-transferase pulldown assays. GST and GST-VP16 TAD fusion protein were expressed in BL21(DE3) *E. coli* cells and purified by glutathione-Sepharose assay (GE Healthcare) after multiple washes with 1 M and 0.5 M NaCl. For whole cell extracts (WCE), HEK293T cells were transfected with plasmid pcDNA4-TO (Invitrogen) harboring either wild-type or mutant Flag-MED25 VBD as per Mirus instructions. 18 h after transfection, cells were harvested with extraction buffer (20 mM Tris-HCl, pH 8.0, 420 mM NaCl, 10% (v/v) glycerol, 0.5% (v/v) NP-40, 0.1 mM NaCl, 1 mM PMSF, 1 mM DTT) for whole cell extract preparation. For pulldown experiments, WCEs were diluted to 100 mM NaCl HEG buffer (20 mM HEPES, pH 7.9, 0.1 mM EDTA, 10% (v/v) glycerol) with 0.01% (v/v) NP-40 to a final protein concentration of 2 μg per μl. 1 mg of WCEs were pre-cleared with glutathione-Sepharose beads for 1 h at 4 °C and then were applied to 50 μl of a 50% slurry of either GST or GST-VP16 TAD beads and incubated at 4 °C for 3 h. Beads were washed six times in 1 ml with 0.4 M KCl HEG buffer with 1% (v/v) NP-40. Bound proteins were eluted with 0.3% (w/v) Sarkosyl.

35. Harper, S.M., Neil, L.C. & Gardner, K.H. Structural basis of a phototropin light switch. *Science* **301**, 1541–1544 (2003).
36. Takeuchi, K., Ng, E., Malia, T.J. & Wagner, G. 1-^{13}C amino acid selective labeling in a ^{2}H^{15}N background for NMR studies of large proteins. *J. Biomol. NMR* **38**, 89–98 (2007).
37. Ferentz, A.E. & Wagner, G. NMR spectroscopy: a multifaceted approach to macromolecular structure. *Q. Rev. Biophys.* **33**, 29–65 (2000).
38. Hiller, S., Ibraghimov, I., Wagner, G. & Orekhov, V.Y. Coupled decomposition of four-dimensional NOESY spectra. *J. Am. Chem. Soc.* **131**, 12970–12978 (2009).
39. Gardner, K.H. & Kay, L.E. Production and incorporation of ^{15}N, ^{13}C, ^{2}H (^{1}H- δ1 methyl) isoleucine into proteins for multidimensional NMR studies. *J. Am. Chem. Soc.* **119**, 7599–7600 (1997).
40. Delaglio, F. *et al.* NMRPipe a Multidimensional Spectra Processing System Based on UNIX Pipes. *J. Biomol. NMR* **6**, 277–293 (1995).
41. Keller, R.L.J. *The Computer Aided Resonance Assignment Tutorial* (Cantina Verlag, 2004).
42. Herrmann, T., Güntert, P. & Wüthrich, K. Protein NMR structure determination with automated NOE-identification in the NOESY spectra using the new software ATNOS. *J. Biomol. NMR* **24**, 171–189 (2002).
43. Shen, Y., Delaglio, F., Cornilescu, G. & Bax, A. TALOS+: a hybrid method for predicting protein backbone torsion angles from NMR chemical shifts. *J. Biomol. NMR* **44**, 213–223 (2009).
44. Brünger, A.T. *et al.* Crystallography & NMR system: A new software suite for macromolecular structure determination. *Acta Crystallogr. D Biol. Crystallogr.* **54**, 905–921 (1998).
45. Gouet, P., Courcelle, E., Stuart, D.I. & Metoz, F. ESPript: analysis of multiple sequence alignments in PostScript. *Bioinformatics* **15**, 305–308 (1999).
46. Bhattacharya, A., Tejero, R. & Montelione, G.T. Evaluating protein structures determined by structural genomics consortia. *Proteins* **66**, 778–795 (2007).

doi:10.1038/nsmb.1999